AIAA JOURNAL
Vol. 44, No. 11, November 2006

Large-Eddy Simulation of Flow over a Wall-Mounted Hump with Separation Control

Donghyun You,* Meng Wang,† and Parviz Moin‡
Stanford University, Stanford, California 94305

DOI: 10.2514/1.21989

Large-eddy simulation with a dynamic subgrid-scale model and nondissipative numerics is employed to predict the turbulent flow separation over a wall-mounted hump and its control. Large-eddy simulation results for the baseline (no control), steady suction, and oscillatory-jet control cases are compared with the results of experimental measurements and previous computational predictions using large-eddy simulation with a constant coefficient Smagorinsky model and dissipative numerics, implicit large-eddy simulation, detached eddy simulation, and unsteady Reynolds-averaged Navier–Stokes simulation. The present large-eddy simulation is shown to be consistently more accurate than the previous numerical approaches in predicting the experimentally measured flow quantities such as the pressure coefficient, reattachment length, mean velocity, and turbulence statistics. It is shown that steady suction and synthetic jet oscillations cause a reduction of the reattachment length by about 12.8 and 7.3%, respectively, compared with the uncontrolled case.

Nomenclature

C	=	hump chord length
C_p	=	surface pressure coefficient
d	=	cavity slot width
f	=	frequency
k	=	turbulent kinetic energy
p	=	pressure
Re	=	Reynolds number
S_{ij}	=	strain rate tensor
t	=	time
U	=	time-averaged streamwise velocity
U_0	=	bulk jet velocity
U_∞	=	inflow free-stream velocity
U_{jet}	=	jet velocity
u	=	streamwise velocity
u_i	=	x_i component of velocity
v	=	wall-normal velocity
w	=	spanwise velocity
x_i	=	Cartesian coordinates
x	=	streamwise coordinate
y	=	wall-normal coordinate
z	=	spanwise coordinate
δ_{ij}	=	Kronecker delta
Δ	=	grid spacing
η	=	cavity slot normal coordinate
ξ	=	cavity slot tangential coordinate
ρ	=	density
τ_{ij}	=	subgrid-scale stress tensor

Superscripts

$\overline{()}$	=	filtered quantity
$+$	=	quantity in wall unit
$'$	=	fluctuation component

I. Introduction

OVER the past several decades various active flow control concepts have been proposed and evaluated to improve the efficiency and stability of aero-/hydrodynamic systems such as turbomachines and road/flight vehicles. Many of these techniques involve continuous blowing or suction, which can produce effective control but is difficult to apply in real fluid systems. In recent years, control devices involving zero-net-mass-flux oscillatory jets or synthetic jets have shown feasibility for industrial applications and effectiveness in controlling flow separation [1–11].

An accurate prediction, not to mention control, of incipient flow separation at high Reynolds numbers is a challenging task for numerical simulations. Recently, a broad range of numerical techniques such as direct numerical simulation (DNS) [6], large-eddy simulation (LES) [7], implicit LES (ILES) [8], detached eddy simulation (DES) [9], and steady or unsteady Reynolds-averaged Navier–Stokes (RANS or URANS) simulations [9–11] have been utilized to predict the turbulent separation and its control over a wall-mounted hump at $Re = 9.36 \times 10^5$, where the Reynolds number is based on C and U_∞. This flow configuration is one of the test cases considered in [2–5]. None of the RANS techniques [2,9–11] gave satisfactory prediction of the important flow features such as the size of the separation bubble, the pressure coefficient on the hump surface, and the mean velocity and turbulence intensity profiles. The DNS results of Postl et al. [6] were unsatisfactory due to the use of unrealistic inflow velocity profiles, insufficient grid resolution, and insufficient spanwise domain size. Morgan et al. [8] obtained better agreement with experimental data using ILES, which relies on numerical dissipation or high-order spatial filtering to play the role of a subgrid-scale model. However, the Reynolds number employed in the ILES is only about one-fifth of the experimental Reynolds number. Although the DES predictions of Krishnan et al. [9] were much better compared with their RANS results, discrepancies with experimental data [3] were still significant. Šarić et al. [7] performed LES with a constant coefficient Smagorinsky model, and reported good predictions in the uncontrolled and steady-suction control cases, but significant deviations of mean velocity profiles from the experimental data [4,5] in the oscillatory jet case. The numerical

Received 22 December 2005; revision received 14 April 2006; accepted for publication 21 April 2006.

*Research Associate, Center for Turbulence Research; dyou@stanford.edu. Member AIAA (corresponding author).

†Senior Research Scientist, Center for Turbulence Research. Currently Associate Professor, Department of Aerospace and Mechanical Engineering, University of Notre Dame, Notre Dame, IN 46556. Member AIAA.

‡The Franklin P. and Caroline M. Johnson Professor of Engineering, Department of Mechanical Engineering, and Director of Center for Turbulence Research and Center for Integrated Turbulence Simulations. Associate Fellow AIAA.

scheme employed in their LES is based on the deferred-correction approach [12], and the numerical dissipation can severely impact the effectiveness of the subgrid-scale model [13].

In this study, we employ LES with a dynamic subgrid-scale model [14] and nondissipative numerics to predict the turbulent flow separation and its control by synthetic jets in the same hump-model configuration. The dynamic subgrid-scale model [14], which has been shown to produce good results in a number of complex turbulent flow simulations [15–19], is employed. In contrast to the LES techniques that employ upwind-biased schemes [7] or the ILES [8], we use an energy-conservative second-order central-difference scheme on a staggered mesh [15,20]. Aliasing errors are controlled by enforcing kinetic energy conservation, not by numerical dissipation or filtering, and artificial damping of small scales is avoided. This feature is particularly important for successful LES of turbulent flows [19,21].

The numerical solutions compared in the present study contain the effects of both the numerical scheme and the turbulence modeling. Therefore, the primary goal of the present study is to examine the predictive capability of a LES technique based on a combination of a nondissipative numerical scheme and a dynamic subgrid-scale model. The present LES has produced superior results compared with those obtained from previous simulations [2,6,8–11] for both controlled and uncontrolled cases. Detailed comparisons of mean and turbulence statistics such as the pressure coefficient, skin-friction coefficients, and velocity and Reynolds stress profiles are presented.

The effects of steady suction and oscillatory jet on flow separation and reattachment are discussed.

II. Computational Methodology

A. Numerical Method

The numerical algorithm and solution methods are described in detail in [20,22], and the main features of the methodology are summarized here. The spatially filtered Navier–Stokes equations for resolved scales in LES are as follows:

$$\frac{\partial \bar{u}_i}{\partial t} + \frac{\partial}{\partial x_j}\bar{u}_i\bar{u}_j = -\frac{\partial \bar{p}}{\partial x_i} + \frac{1}{Re}\frac{\partial}{\partial x_j}\frac{\partial \bar{u}_i}{\partial x_j} - \frac{\partial \tau_{ij}}{\partial x_j} \tag{1}$$

$$\frac{\partial \bar{u}_i}{\partial x_i} = 0 \tag{2}$$

where τ_{ij} is the subgrid-scale (SGS) stress tensor. All the coordinate variables, velocity components, and pressure are nondimensionalized by the hump chord length C, the inflow free-stream velocity U_∞, and ρU_∞^2, respectively. The time is normalized by C/U_∞. The governing equations (1) and (2) are rewritten in a conservative form in generalized coordinates in two directions and a Cartesian coordinate in the third (spanwise) direction. The dependent variables in the transformed Navier–Stokes equations are volume fluxes across the faces of computational cells, which are equivalent to the use of the contravariant velocity components on a staggered grid multiplied by the Jacobian of the coordinate transformation. With this choice of variables, the discretized mass conservation can easily be satisfied. The key feature of the numerical method is the use of a nondissipative, central-difference spatial discretization scheme which has been demonstrated to be crucial for retaining the accuracy and predictive capability of the LES [19].

The SGS stress tensor τ_{ij} is modeled by a Smagorinsky type eddy-viscosity model:

$$\tau_{ij} - \tfrac{1}{3}\delta_{ij}\tau_{ij} = -2c\Delta^2|\bar{S}|\bar{S}_{ij} \tag{3}$$

The Smagorinsky coefficient c is dynamically computed employing the procedure proposed by Germano et al. [14] with the modification by Lilly [23]. It has been reported that the modified procedure based on a least-square optimization of the stress-strain relationship enhances the numerical stability and improves the solution [23,24].

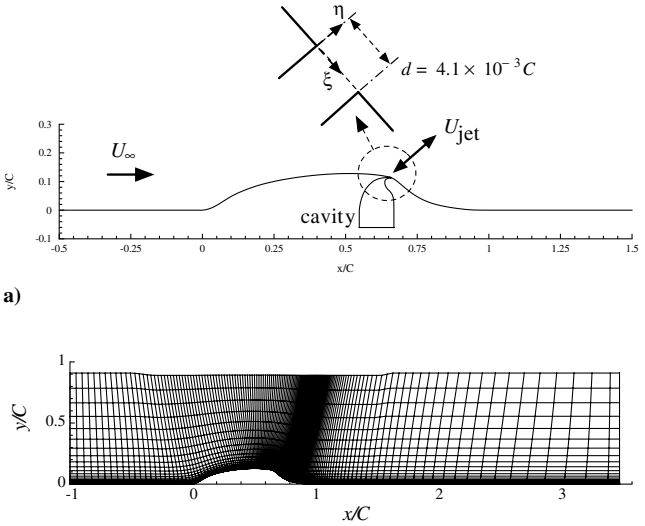

Fig. 1 a) Flow configuration for experimental study of flow over a wall-mounted hump and b) computational domain and mesh in the x–y plane ($\frac{1}{5}$ mesh lines plotted).

The temporal integration method used to solve the transformed governing equations is based on a fully implicit fractional step method which avoids the severe time-step restriction that would occur in the synthetic jet orifice region with an explicit scheme. All terms including cross-derivative diffusion terms are advanced using the Crank–Nicolson method in time and are discretized by the second-order central difference in space. A Newton iterative method is used to solve the discretized nonlinear equations. The Poisson equation is solved by a hybrid procedure which applies a multigrid method to the curvilinear planes and a Fourier spectral method to the remaining Cartesian direction.

The code is parallelized using message passing directives (OpenMP) for shared memory platforms like SGI Origin 2000/3800 and Compaq GS320. It achieves a high level of parallel performance by utilizing cache-management strategies and minimizing data dependency [22].

B. Flow Configuration

The flow configuration is shown in Fig. 1 along with a two-dimensional slice of the computational grid with only one in every five grid lines plotted for clarity. This configuration is the third test case considered in [2–5]. It is based on the original experiment of Seifert and Pack [3] which was later repeated by Greenblatt et al. [4,5] to provide a complete data set for CFD validations. In the present LES, the experimental data provided by Greenblatt et al. [4,5] is used for validation. The hump is the upper surface of a Glauert–Goldschmied type airfoil and has a chord length of $C = 0.42$ m, a maximum height of 0.0537 m, and a span of 0.5842 m. A cavity slot is located at approximately 65% chord and is used for producing a steady suction and a zero-efflux oscillatory jet. The boundary layer first experiences an adverse pressure gradient as it approaches the hump. It then accelerates over the front convex portion of the hump where the pressure gradient turns favorable and separates over a relatively short concave section in the aft region due to the strong adverse pressure gradient.

The computational domain is of size $L_x \times L_y \times L_z = 4.5C \times 0.9C \times 0.2C$. It is smaller than the test section of the experiment in the streamwise and spanwise directions to reduce the computational cost. The present spanwise domain size $L_z = 0.2C$, which corresponds to about 3 inflow boundary layer thickness, has been subsequently determined from the information obtained from a prior simulation that was performed with the spanwise domain size of $0.15C$. It was confirmed that results were relatively insensitive to the spanwise domain size bigger than $0.15C$. Figure 2 is the example of the study, which shows reasonable robustness of the surface

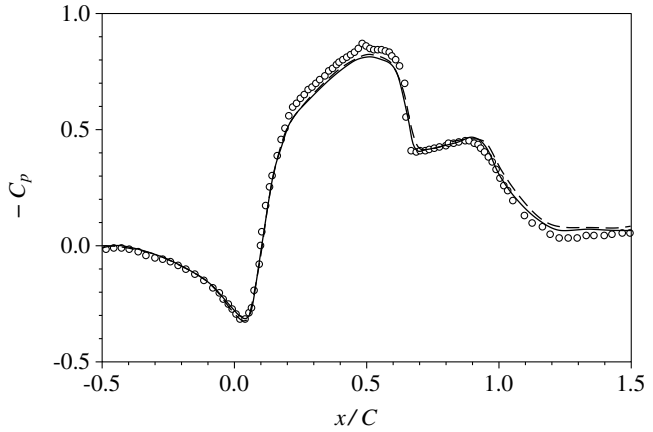

Fig. 2 Surface pressure coefficient for the baseline case. Solid line: present LES with $L_z = 0.2C$ and 721 × 161 × 65 mesh; dashed line: present LES with $L_z = 0.15C$ and 721 × 161 × 48 mesh; open circles: experiment [4].

pressure coefficient in the baseline case with respect to the spanwise domain size. The top-wall boundary is located at $y/C \approx 0.9$ with a slight variation to account for the side-wall blockage effect in the experiment.[§] The Reynolds number of this flow is 9.36×10^5 based on the hump chord and inflow free-stream velocity.

A small slot of width $d = 4.1 \times 10^{-3}C$ across the entire length of the span and located at approximately 65% of the hump chord is used to introduce flow control, using either steady suction with bulk suction velocity $U_0 = 0.37U_\infty$ or sinusoidal suction/blowing at nondimensional frequency of $f = 1.6812U_\infty/C$ with peak bulk jet velocity of $U_0 = 0.77U_\infty$. Velocity boundary conditions applied at the slot opening are used to model the control jets generated by the cavity. Parabolic velocity profiles

$$U_{\text{jet}} = 6U_0\left[\frac{\xi}{d} - \left(\frac{\xi}{d}\right)^2\right] \tag{4}$$

and

$$U_{\text{jet}} = 6U_0\left[\frac{\xi}{d} - \left(\frac{\xi}{d}\right)^2\right]\sin(2\pi ft) \tag{5}$$

where $0 \le \xi \le d$, are used in the direction η normal to the slot (see Fig. 1 for definitions of ξ and η coordinates), for steady suction and sinusoidal oscillatory jet, respectively. There is a consensus among previous investigators [2,7,10] that the control effects on the hump flow are mostly unaffected by using such velocity boundary conditions instead of simulating the detailed cavity flow for the suction and synthetic jets. Following the experimental values, a mass flux coefficient of 0.15% is used for the steady suction case. For the oscillatory-jet case, a momentum coefficient of 0.11% based on the peak jet velocity is used.

No-stress and no-slip boundary conditions are applied along the top and bottom walls, respectively. Periodic boundary conditions are used along the spanwise (z) direction. The inflow turbulent boundary layer data are provided from a separate simulation of flat-plate boundary layer using the method of Lund et al. [25] with a boundary layer thickness of $\delta = 0.073C$ at $x/C = -2.14$ as in the experiment. At the exit boundary, the convective boundary condition is applied, with the convection speed determined by the streamwise velocity averaged across the exit plane.

The mesh size used for the present simulation is $721 \times 161 \times 65(x \times y \times z)$. 24 mesh points are allocated along the cavity slot. The grid spacings on the wall in the streamwise, wall-normal, and spanwise directions are $\Delta x/C \le 4.1 \times 10^{-2}$, $\Delta y/C \le 1.74 \times 10^{-5}$, and $\Delta z/C \le 3.1 \times 10^{-3}$, respectively. The wall resolution is within the range $\Delta x^+ \le 50$, $\Delta y^+ \le 0.8$, and $\Delta z^+ \le 25$. The present resolution is similar to or better than that found in a number of successful LES of separated flows using the present code [15–17,19]. Before this simulation, coarser grid simulations were carried out to determine the resolution requirements, and the final mesh was subsequently constructed using this information.

The simulation is advanced in time with maximum Courant–Friedrichs–Lewy number equal to 3, which corresponds to $\Delta tU_\infty/C \approx 0.4 \times 10^{-3}$. Each time step requires a wallclock time of about 20 sec when 8 CPUs of IBM p690 are used. The present results are obtained by integrating the governing equations over an interval of about $10C/U_\infty$.

III. Results and Discussion

LES results for the baseline (no control), suction, and oscillatory-jet cases are compared with those provided by the experiment [4,5], previous LES of Šarić et al. [7], ILES [8], DES [9], and URANS [10]. Except for the ILES, the previous numerical studies [7,9,10] provide only a subset of data with which the present LES results are compared. For instance, only the pressure coefficient is available for the oscillatory case in the URANS. A number of (U)RANS calculations have been made by different researchers [e.g., [9–11]; see also [2] for a summary of (U)RANS studies], and their results are qualitatively similar. Here, we use those in Capizzano et al. [10] as representative solutions for comparison.

Figure 3 shows comparisons of the mean surface pressure coefficients $-C_p$, which reflect overall features of the flowfield. The flow is accelerated up to about the midchord of the hump, where a peak magnitude of $-C_p$ is observed. A sudden drop of $-C_p$ afterwards leads to separation at around $x/C = 0.65$, which corresponds to the location of the cavity slot. All the numerical simulations, including the present LES, LES of Šarić et al., ILES, DES, and URANS, predict reasonably well the hump surface pressure distribution up to the separation point for uncontrolled and controlled cases. Continuous suction and oscillatory jets shorten the recirculation bubble size relative to the uncontrolled case. The superior predictive capability of the present LES is noticeable after the flow separation, where URANS [10] was clearly unable to predict the pressure recovery and the correct separation bubble size. The ILES [8] shows much better results than does URANS but still deviates from the experimental measurement in the oscillatory case. Morgan et al. [8] suggested that the lower Reynolds number in the ILES reduces the effectiveness of flow control. DES and the LES of Šarić et al. also show significant errors for the steady suction case.

Gross features of the flow separation in the uncontrolled and controlled cases are visualized using the spanwise vorticity contours as shown in Fig. 4. The incoming turbulent boundary layer separates due to the strong adverse pressure gradient near the cavity slot and produces abundant small scale vortices between the separated shear layer and bottom wall [Fig. 4a]. In Fig. 4b, it is clear that steady suction weakens the shear layer and reduces the separation bubble size by removing mass flux through the cavity slot. In the oscillatory-jet case shown in Fig. 4c, a periodic production and convection of large-scale vortices is observed. The repeated process of vortex roll-up and shedding is also found to reduce effectively the separation bubble size. A comparison of the time-averaged separation bubble sizes predicted by the present LES for the three cases is made in Fig. 5, which also shows qualitatively the effectiveness of control jets in terms of the flow separation and reattachment locations and bubble size. Both the steady suction and oscillatory jets are found to reduce the size of the separation bubble and move the core of flow recirculation upstream.

The effectiveness of steady suction and oscillatory jet on separation control is more clearly illustrated in Fig. 6, which shows a comparison of the skin-friction coefficients C_f predicted by the present LES for the uncontrolled and controlled cases. The line $C_f = 0$ delineates separated flow from attached and reattached flow. In the baseline case, the LES shows favorable agreement with experimental data except for the front convex region of the hump. The reattachment locations obtained from the present LES are

[§]As recommended at http://cfdval2004.larc.nasa.gov/case3.html [cited 01 October 2005].

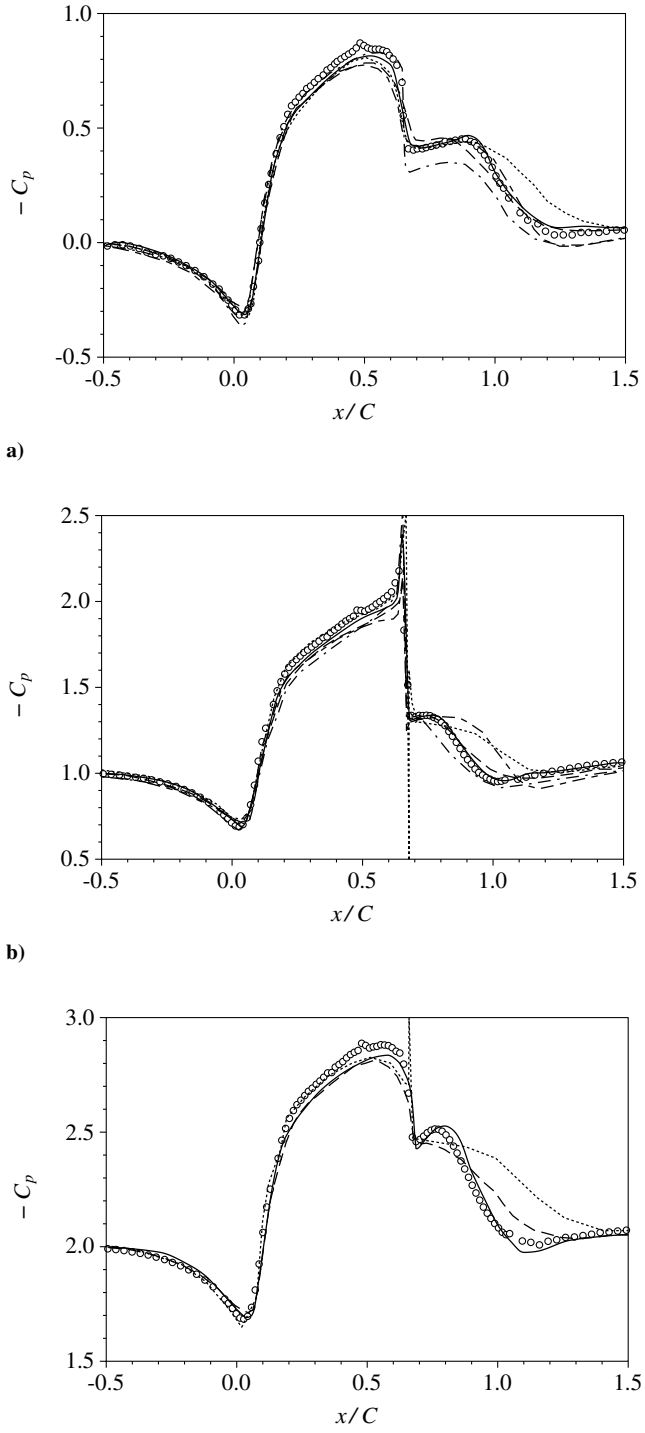

Fig. 3 Surface pressure coefficient for a) baseline, b) steady-suction, and c) oscillatory-jet cases. Solid line: present LES; dash–dotted line: LES of Šarić et al. [7]; dashed line: ILES [8]; dash–short-dashed line: DES [9]; dotted line: URANS [10]; open circles: experiment [4,5].

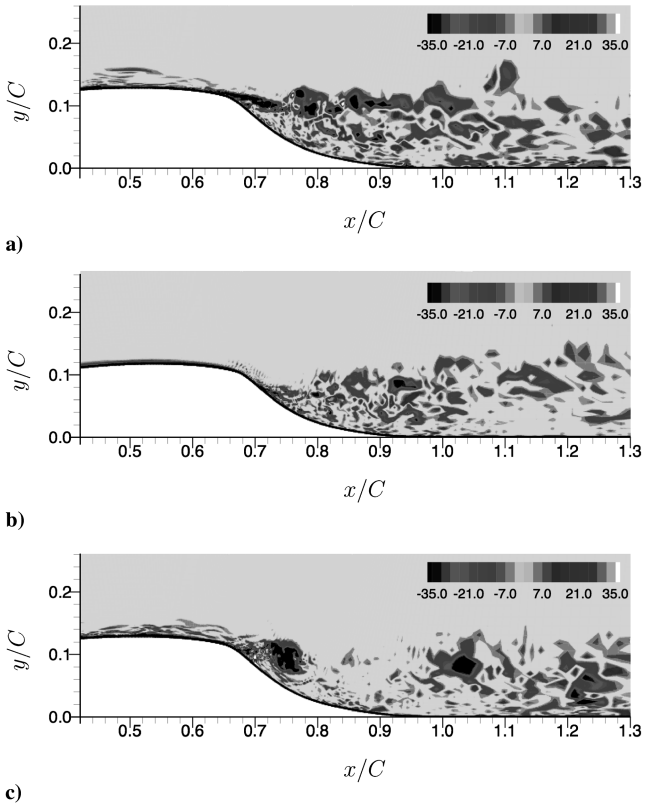

Fig. 4 Instantaneous spanwise vorticity contours. a) Baseline; b) steady suction; c) oscillatory jet. Twenty contour levels in the range of ±35 are plotted.

quantitatively compared in Table 1 to experimental and other numerical results for the three cases. The present LES and the LES of Šarić et al. [7] yield more accurate predictions of the separation bubble sizes than other previous numerical results. Although the ILES [8] gives favorable agreement with experiments for the baseline and steady-suction cases, the reattachment length is approximately 10% longer in the oscillatory case. As observed earlier in the surface pressure distributions, the URANS calculations gave significantly longer reattachment lengths for all three cases. The deficiency of URANS is more clear in the case of oscillatory jet control. In general, RANS models are known to have difficulty in predicting flow separation and unsteady mixing [2].

In Fig. 7, the uncontrolled and controlled mean streamwise velocity profiles are compared with experimental and other numerical data at two streamwise locations, $x/C = 0.8$ and 1.2. Note that not all the mean velocity and turbulence statistics at those two locations are available from other numerical solutions with which the present LES results are compared. Inside the separation bubble at $x/C = 0.8$, the LES profiles show best match with the experimental data, although other numerical simulations also show favorable agreements. The velocity profiles indicate that the separation bubble is decreased by both the steady suction and oscillation. In relative terms, the suction is more effective than the oscillatory jet in reducing the separation bubble size, as also shown in Figs. 5 and 6 and Table 1. At a location slightly downstream of flow reattachment ($x/C = 1.2$), the agreement between the present LES and experimental data is quite good, whereas the LES of Šarić et al. [7] and DES [9] could not correctly predict the velocity profiles in the oscillatory jet and suction cases, respectively. The predictions of Šarić et al. are comparable to the present LES results in the baseline and steady suction cases. The DES produces a marginal result in the baseline case, but fails to predict the mean velocity profile in the suction case. The ILES and URANS show profiles that are not as fully recovered as in the experiment due to delayed reattachment.

Table 1 Locations (x/C) of flow reattachment behind the hump

Case	Baseline	Suction	Oscillation
Present LES	1.09	0.95	1.01
LES of Šarić et al. [7]	1.114	0.947	1.020
ILES[a] [8]	1.127	0.984	1.097
DES [9]	1.13		
URANS [10]	1.25	1.08	1.15
Experiment [4,5]	1.110 ± 0.003	0.94 ± 0.05	0.98

[a]A lower Reynolds number of $Re = 2 \times 10^5$ is used in the ILES.

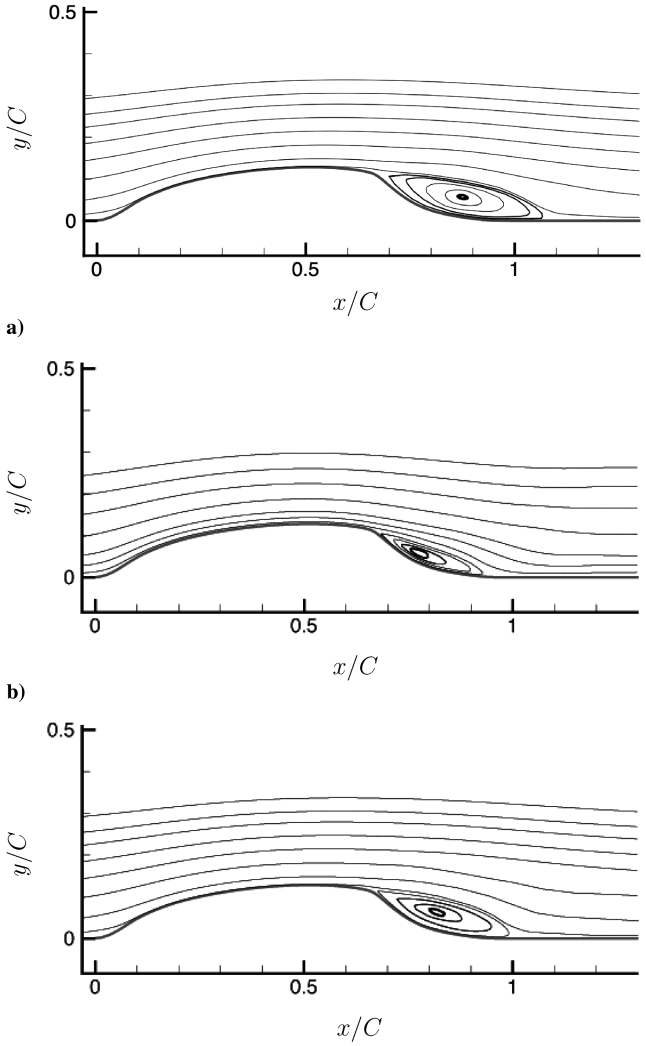

Fig. 5 Mean streamlines from the present LES. a) Baseline; b) steady suction; c) oscillatory jet.

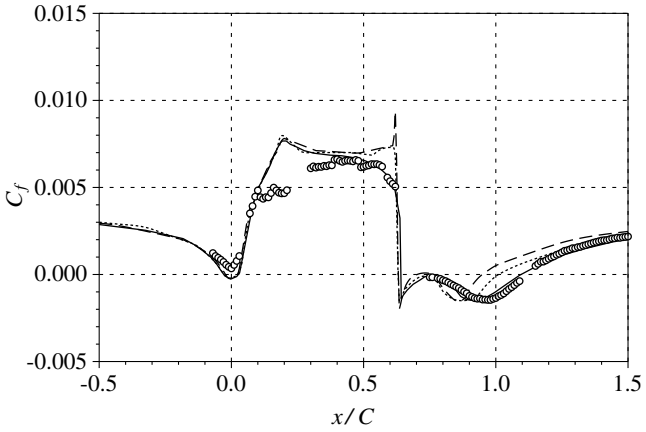

Fig. 6 Skin-friction coefficient. Lines are from the present LES and symbol is from the experiment [4]. Solid line, open circles: baseline; dashed line: steady suction; dotted line: oscillatory jet.

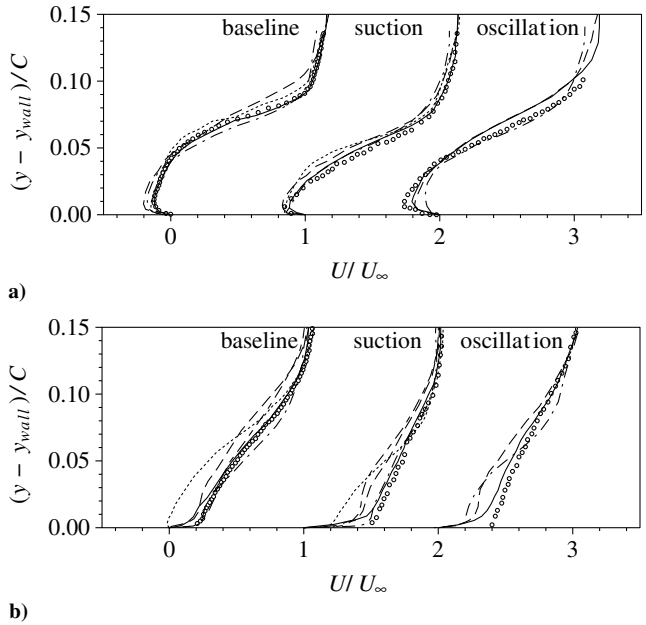

Fig. 7 Mean streamwise velocity profiles at a) $x/C = 0.8$ and b) $x/C = 1.2$. Solid line: present LES; dash–dotted line: LES of Šarić et al. [7]; dashed line: ILES [8]; dash–short-dashed line: DES [9]; dotted line: URANS [10]; open circles: experiment [4,5]. The profiles for the suction and oscillation cases are shifted by 1 and 2, respectively.

Overall, the streamwise velocity profiles are fuller in the cases with flow control and are the fullest in the suction case due to the earliest flow reattachment.

Comparisons of turbulent kinetic energy (TKE) obtained from the present LES and other numerical and experimental studies are shown in Fig. 8 at the same two streamwise locations, $x/C = 0.8$ and 1.2, where the mean streamwise velocity profiles are compared. The superior predictive capability of the present LES is again evident. For uncontrolled and controlled cases, the LES results agree reasonably well with the experimental data and are better than those from ILES and URANS. The ILES shows a reasonable agreement with the experimental data in the controlled cases, but worse results than URANS in the baseline case. No TKE data were presented by Šarić et al. from their LES. Inside the separation bubble, the peak TKE is found closer to the wall in the suction and oscillatory cases compared with the baseline case. This is an indication of the control effect on the turbulent mixing. Larger TKE is observed inside the bubble than in the reattached region downstream. At $x/C = 1.2$, larger TKE magnitudes are found in the baseline and oscillatory cases than in the suction case, which is related to the larger sizes of the separation bubbles in the former cases.

The resolved Reynolds stress profiles from numerical simulations and experiments are compared in Fig. 9. The present LES is consistently better in predicting the Reynolds shear stress in the uncontrolled and controlled cases. The LES results of Šarić et al. [7] deviate from the experimental data in the baseline case, but are in good agreement with experimental data in the suction case. It is well known that a constant subgrid-scale model coefficient, which was employed by Šarić et al. [7] and the numerical dissipation present in their scheme both affect the robustness of the LES solutions in various flow situations [14]. Figure 10 shows time- and spanwise-averaged dynamic Smagorinsky model coefficients predicted by the present dynamic procedure in the x–y plane and clearly indicates a nonuniform distribution of the Smagorinsky model coefficients across the flowfield. The URANS results significantly under-predict the peak magnitude of the Reynolds shear stress, particularly inside the separation bubble. This under-prediction is consistent with the delayed reattachment, since it indicates reduced turbulent mixing inside the separated region. The results from ILES are consistent with its turbulent kinetic energy predictions, showing better agreements with experimental data in the controlled cases and poor agreement in the baseline case. However, these results are difficult to interpret given that the simulations were conducted at a reduced Reynolds number.

IV. Conclusions

Large-eddy simulations with a dynamic subgrid-scale model and nondissipative numerics have been employed to predict the turbulent

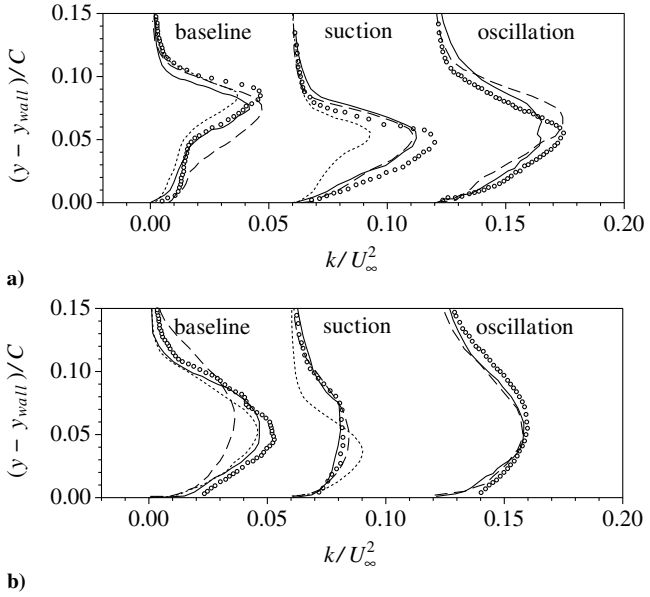

Fig. 8 Turbulent kinetic energy profiles at a) $x/C = 0.8$ and b) $x/C = 1.2$. Solid line: present LES; dashed line: ILES [8]; dotted line: URANS [10]; open circles: experiment [4,5] . The profiles for the suction and oscillation cases are shifted by 0.06 and 0.12, respectively.

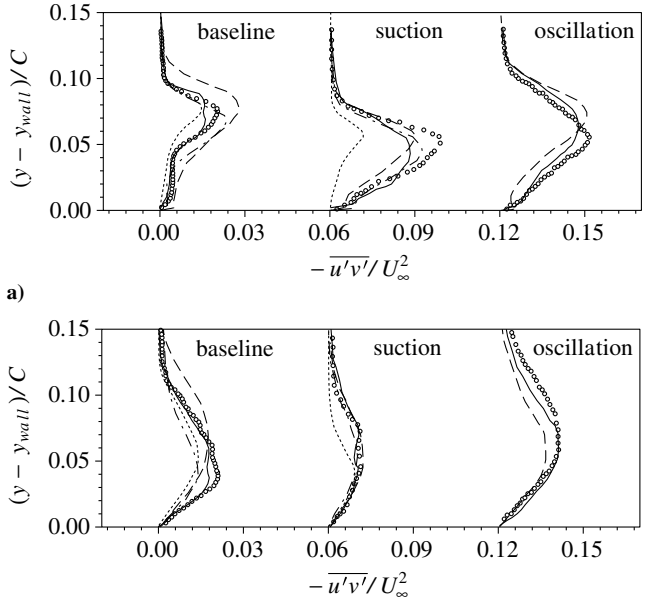

Fig. 9 Reynolds shear stress profiles at a) $x/C = 0.8$ and b) $x/C = 1.2$. Solid line: present LES; dash–dotted line: LES of Šarić et al. [7]; dashed line: ILES [8]; dotted line: URANS [10]; open circles: experiment [4,5]. The profiles for the suction and oscillation cases are shifted by 0.06 and 0.12, respectively.

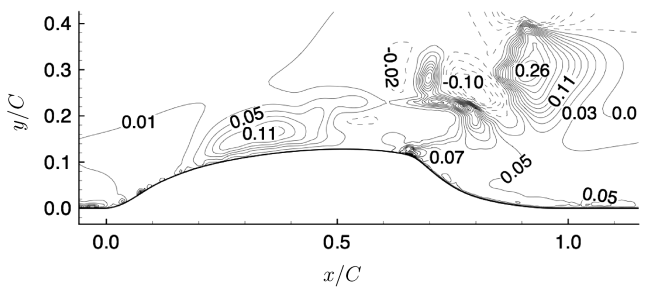

Fig. 10 Contour plot of time- and spanwise-averaged dynamic Smagorinsky model coefficient (c) in the x–y plane. Twenty contour levels in the range of $-0.1 \sim 0.3$ are plotted. Negative values are dashed.

flow separation over a wall-mounted hump and its control by steady-suction and zero-net-mass-flux oscillatory jets. Results from the present LES for the uncontrolled and controlled cases are compared with experimental data and previous computational predictions using LES with a constant coefficient Smagorinsky model and dissipative numerics, implicit LES, DES, and URANS. The present LES is shown to be consistently more accurate than the previous numerical approaches. It predicts well the experimentally measured flow quantities such as the pressure coefficient, reattachment length, mean velocity, and turbulence statistics. The reattachment points downstream of the hump are predicted accurately for all three cases. It is also shown that steady-suction and synthetic jet oscillations cause a reduction of the reattachment length by $7 \sim 13\%$, compared with the uncontrolled case.

Acknowledgments

The authors acknowledge support from the Boeing Company and the valuable discussions with Arvin Shmilovich.

References

[1] Glezer, A., and Amitay, M., "Synthetic Jets," *Annual Review of Fluid Mechanics*, Vol. 34, 2002, pp. 503–529.

[2] Rumsey, C. L., Gatski, T. B., Sellers, W. L., III, Vatsa, V. N., and Viken, S. A., "Summary of the 2004 CFD Validation Workshop on Synthetic Jets and Turbulent Separation Control," AIAA Paper 2004-2217, June 2004.

[3] Seifert, A., and Pack, L. G., "Active Flow Separation Control on Wall-Mounted Hump at High Reynolds Numbers," *AIAA Journal*, Vol. 40, No. 7, 2002, pp. 1363–1372.

[4] Greenblatt, D., Paschal, K. B., Yao, C.-S., Harris, J., Schaeffler, N. W., and Washburn, A. E., "A Separation Control CFD Validation Test Case Part 1: Baseline and Steady Suction," AIAA Paper 2004-2220, June 2004.

[5] Greenblatt, D., Paschal, K. B., Yao, C.-S., and Harris, J., "A Separation Control CFD Validation Test Case Part 2: Zero Efflux Oscillatory Blowing," AIAA Paper 2005-0485, January 2005.

[6] Postl, D., Wernz, S., and Fasel, H., "Case 3: Direct Numerical Simulation on the Cray X1," *NASA Langley Workshop on CFD Validation of Synthetic Jets and Turbulent Separation Control*, 2004, pp. 3.3.1–3.3.5.

[7] Šarić, S., Jakirlić, S., and Tropea, C., "Computational Analysis of Locally Forced Flow over a Wall-Mounted Hump at High-Re Number," *Fourth International Symposium on Turbulence and Shear Flow Phenomena*, edited by J. A. C. Humphrey, J. K. Eaton, R. Friedrich, N. Kasagi, M. A. Leschziner, and T. B. Gatski, June 2005, pp. 1189–1194.

[8] Morgan, P. E., Rizzetta, D. P., and Visbal, M. R., "Large-Eddy Simulation of Separation Control for Flow over a Wall-Mounted Hump," AIAA Paper 2005-5017, June 2005.

[9] Krishnan, V., Squires, K. D., and Forsythe, J. R., "Prediction of Separated Flow Characteristics over a Hump Using RANS and DES," AIAA Paper 2004-2224, June 2004.

[10] Capizzano, F., Catalano, P., Marongiu, C., and Vitagliano, P. L., "U-RANS Modelling of Turbulent Flows Controlled by Synthetic Jets," AIAA Paper 2005-5015, June 2005.

[11] Morgan, P. E., Rizzetta, D. P., and Visbal, M. R., "Numerical Investigation of Separation Control for Flow over a Wall-Mounted Hump," AIAA Paper 2004-2510, June 2004.

[12] Khosla, P. K., and Rubin, S. G., "A Diagonally Dominant Second-Order Accurate Implicit Scheme," *Computers and Fluids*, Vol. 2, No. 2, 1974, pp. 207–209.

[13] Ghosal, S., "An Analysis of Numerical Errors in Large-Eddy Simulations of Turbulence," *Journal of Computational Physics*, Vol. 125, No. 1, 1996, pp. 187–206.

[14] Germano, M., Piomelli, U., Moin, P., and Cabot, W. H., "A Dynamic Subgrid-Scale Eddy-Viscosity Model," *Physics of Fluids A*, Vol. 3, No. 7, 1991, pp. 1760–1765.

[15] You, D., Mittal, R., Wang, M., and Moin, P., "Computational Methodology for Large-Eddy Simulation of Tip-Clearance Flows," *AIAA Journal*, Vol. 42, No. 2, February 2004, pp. 271–279.

[16] Wang, M., and Moin, P., "Computation of Trailing-Edge Flow and Noise Using Large-Eddy Simulation," *AIAA Journal*, Vol. 38, No. 12, 2000, pp. 2201–2209.

[17] Kaltenbach, H.-J., Fatica, M., Mittal, R., Lund, T. S., and Moin, P., "Study of Flow in a Planar Asymmetric Diffuser Using Large-Eddy Simulation," *Journal of Fluid Mechanics*, Vol. 390, July 1999, pp. 151–

185.
[18] Wu, X., and Squires, K. D., "Numerical Investigation of the Turbulent Boundary Layer over a Hump," *Journal of Fluid Mechanics*, Vol. 362, May 1998, pp. 229–271.
[19] Mittal, R., and Moin, P., "Suitability of Upwind-Biased Schemes for Large-Eddy Simulation of Turbulent Flows," *AIAA Journal*, Vol. 36, No. 8, 1997, pp. 1415–1417.
[20] Choi, H., Moin, P., and Kim, J., "Turbulent Drag Reduction: Studies of Feedback Control and Flow Over Riblets," Stanford University, Report TF-55, Department of Mechanical Engineering, Stanford, California, September 1992.
[21] Beaudan, P., and Moin, P., "Numerical Experiments on the Flow Past A Circular Cylinder at Sub-Critical Reynolds Number," Stanford University, Report TF-62, Department of Mechanical Engineering, Stanford, California, December 1994.
[22] You, D., Moin, P., Wang, M., and Mittal, R., "Study of Tip Clearance Flow in a Turbomachinery Cascade Using Large Eddy Simulation," Stanford University, Report TF-86, Department of Mechanical Engineering, Stanford, California, May 2004.
[23] Lilly, D. K., "A Proposed Modification of the Germano Subgrid-Scale Closure Model," *Physics of Fluids A*, Vol. 4, No. 3, 1992, pp. 633–635.
[24] Spyropoulos, E. T., and Blaisdell, G. A., "Evaluation of the Dynamic Model for Simulations of Compressible Decaying Isotropic Turbulence," *AIAA Journal*, Vol. 34, No. 5, 1996, pp. 990–998.
[25] Lund, T. S., Wu, X., and Squires, K. D., "Generation of Turbulent Inflow Data for Spatially Developing Boundary Layer Simulations," *Journal of Computational Physics*, Vol. 140, No. 2, 1998, pp. 233–258.

P. Givi
Associate Editor